



Article

Differences in the Electric Field Distribution Predicted with a Mathematical Model of Cylindrical Electrodes of Finite Length vs. Infinite Length: A Comparison Based on Analytical Solution

Ricardo Romero-Mendez ^{1,*}  and Enrique Berjano ² 

¹ Facultad de Ingeniería, Universidad Autónoma de San Luis Potosí, Zona Univeristaria, San Luis Potosí 78290, Mexico

² BioMIT, Department of Electronic Engineering, Universitat Politècnica de València, Camino de Vera, 46022 Valencia, Spain; eberjano@eln.upv.es

* Correspondence: rromerom@uaslp.mx

Abstract: Cylindrical-shaped metal electrodes are used in numerous medical specialties to force an electric field into the surrounding tissue (e.g., in electrical stimulation and electroporation). Although these electrodes have a limited length in reality, previous mathematical modeling studies have simplified the physical situation and have built a model geometry based on a cylindrical electrode of infinite length, which allows for reducing the model from 2D to 1D. Our objective was to quantify the differences in the electric field values between the finite and infinite electrode cases and assess the adequacy of the mentioned simplification for different values of electrode diameter and length. We used analytical solutions for the electric field distribution. We found that the electric field distribution is substantially different for both cases, not only near the edges of the electrode (when finite length is assumed) and in close locations (<1 mm), but even in the central area and at distances greater than 2 mm. Our work presents analytical solutions for both cases (finite and infinite length), which, despite the oscillations derived from computational limitations, could be used by researchers involved in electric field modeling in biological tissues, in order to quantify the possible error generated with simple models in geometric terms that assume infinite length.



Citation: Romero-Mendez, R.; Berjano, E. Differences in the Electric Field Distribution Predicted with a Mathematical Model of Cylindrical Electrodes of Finite Length vs. Infinite Length: A Comparison Based on Analytical Solution. *Mathematics* **2023**, *11*, 4447. <https://doi.org/10.3390/math11214447>

Academic Editor: Jacques Lobry

Received: 27 September 2023

Revised: 16 October 2023

Accepted: 25 October 2023

Published: 27 October 2023



Copyright: © 2023 by the authors. Licensee MDPI, Basel, Switzerland. This article is an open access article distributed under the terms and conditions of the Creative Commons Attribution (CC BY) license (<https://creativecommons.org/licenses/by/4.0/>).

Keywords: analytical solution; cylindrical electrode; electrical problem; electroporation; electrical stimulation

MSC: 35Q60; 78M99

1. Introduction

Cylindrical-shaped metal electrodes are used in numerous medical specialties to force an electric field into the surrounding media (biological tissue and cell suspension), for example, in electrical stimulation [1] and electroporation [2]. In other cases, such as in radiofrequency ablation, the electric field is induced to create an electrical current and provoke a localized Joule heating [3]. These electrodes consist of a cylindrical metal piece partially coated with plastic. The electrode is really the exposed part, i.e., the uninsulated portion, also known as contact (Figure 1A). During clinical use, the exposed part is completely surrounded by tissue. To create the electric field, a voltage difference has to be set between two electrodes: one of which is the cylindrical electrode itself (active electrode) and the other is a large area electrode, also known as a patch, reference electrode, returning electrode, or dispersive electrode, which is placed far from the active electrode.

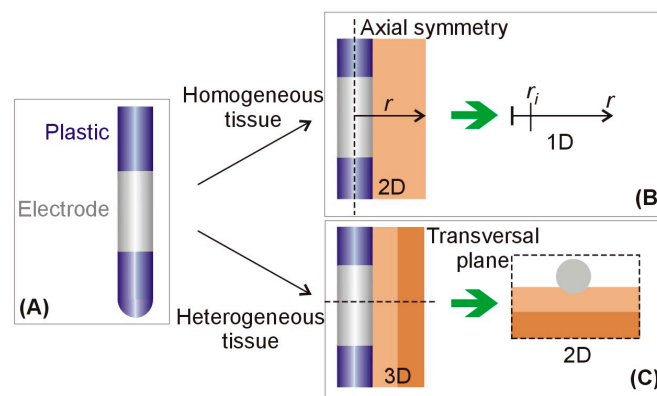


Figure 1. (A) Metal cylindrical electrode attached to two plastic segments. (B) When the cylindrical electrode is assumed to have infinite length, and the surrounding tissue is homogeneous, the model geometry can be simplified from 2D to 1D since only the radial coordinate is relevant. (C) When the surrounding tissue is heterogeneous, the model geometry can be simplified from 3D to 2D by also considering an infinite-length electrode, specifically via extrusion from a transverse plane.

The length of the cylindrical electrodes is limited to a few millimeters in most clinical applications, e.g., 1.5–2.4 mm in the case of brain stimulation to detect epileptic foci [4] and 3–4 mm in the case of electroporation of myocardium to treat cardiac arrhythmias [2]. Although in reality, cylindrical electrodes have a limited length, some previous studies have simplified the physical situation and have built a model geometry based on a cylindrical electrode of infinite length [3,5–7]. Assuming an infinite length for a very thin cylindrical electrode (i.e., needle type) is an approximation previously used in the calculation of the forced electric field between different electrode spatial arrangements, not necessarily between an electrode and a patch located in the distance (i.e., monopolar mode) [8,9]. This allows for reducing the model from 2D to 1D in the case of contiguous homogeneous tissue (see Figure 1B) [3,5] and from 3D to 2D in the case of heterogeneous tissue by establishing a cutting plane in the center of the electrode (see Figure 1C) [6,7]. The justification for this simplification is the assumption that the electric field for the infinite-length case will be very similar to that generated with the finite-length case at least in the central zone of the electrode, i.e., far from the edges where it is known that the value of electric field presents extremely high values due to the high voltage gradient [10]. As far as we know, there are no studies regarding the quantification of the electric field differences in both cases.

Our objective was to quantify the differences in the electric field distributions predicted with the mathematical models considering finite vs. infinite length of cylindrical electrodes rounded by biological tissue and hence assess the adequacy of the mentioned approximation (i.e., model based on infinite length) for different values of electrode diameter and length. To this end, we used analytical solutions for the electric field previously obtained in the case of homogeneous tissue, specifically, a 1D model that assumes an infinite-length electrode [11] and a 2D model that assumes a finite-length electrode [12]. In contrast to the use of numerical techniques (such as the finite element method and finite difference method), the use of exact solutions is indispensable to validate numerical codes, since the mesh refinements used in the codes should be able to capture the large gradients of voltage and electric field around the cylindrical electrode, which should be accurately determined using the analytical solution. These analytical solutions, even simplifying reality by assuming uniform biological tissue, allow the numerical solutions to be verified [8,13]. Once verified, solutions based on numerical methods, such as the finite element method, are used in the case of heterogeneous tissues, whose analytical solution is highly complex [14].

2. Methods

2.1. Model Geometry

The analytical model represents a physical situation in which a cylindrical electrode with radius r_i and length z_0 is completely surrounded by homogeneous tissue (Figure 2A). The dispersive electrode is located far from the cylindrical electrode and has a comparatively much larger area. As the electrode radius is much smaller than the tissue dimensions, we assume the domain comprises an annular section of tissue with height $z_0 = 210$ mm with inner radius r_i and outer radius r_o . The device has several active electrode sections followed by insulated plastic strips. In the study that follows, we considered a model including three active electrode sections but only plotted the section shown in paler pink in Figure 2A, plotting using a local coordinate \bar{z} , because symmetry conditions in the planes that cut the insulated sections in their mid-length. The relevant parameters of the electrode and solution domain for the 2D problem are the length of the active sections of the electrode, $L = z_2 - z_1 = z_4 - z_3 = z_6 - z_5$; the length of the insulated sections of the electrode that separate the active sections, $S = 2z_1 = z_3 - z_2 = z_5 - z_4$; the external radius of the electrode, r_i ; the radial dimension of the domain, r_o ; and the height of the domain, z_0 . The distance $z_0 - z_6$ adjusts itself to the other parameters, such that only three sections of the active electrode are allowed in the domain.

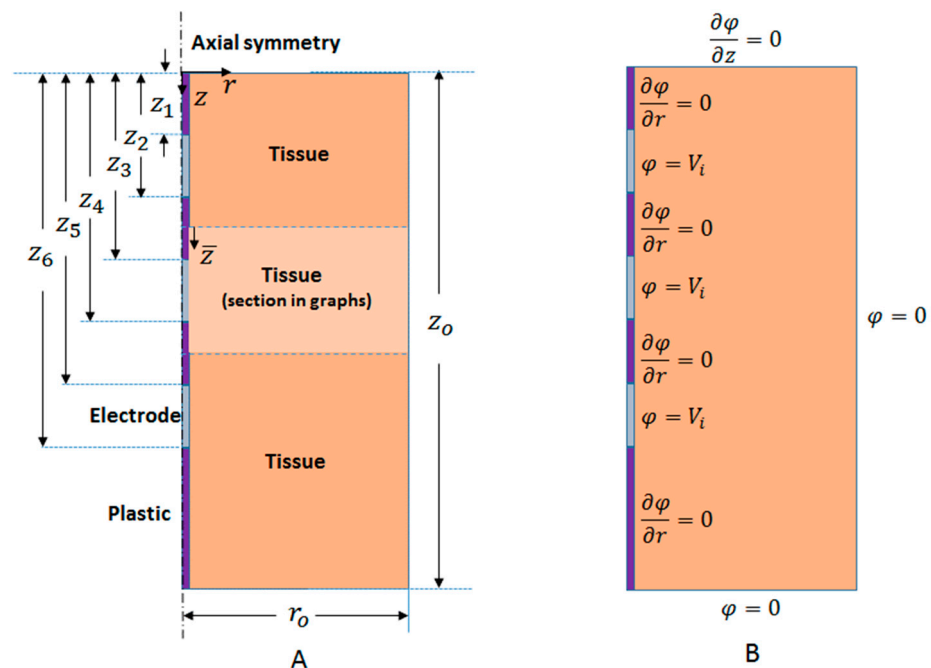


Figure 2. (A) The two-dimensional model for a cylindrical electrode with finite length z_0 . There is axial symmetry around the electrode axis. The outer dimensions are radius r_o and height z_0 . (B) Boundary conditions for the electrical problem.

2.2. Governing Equations and Boundary Conditions

The Laplace equation represents the electrical problem mathematically as follows:

$$\nabla(\sigma \nabla \varphi) = 0 \tag{1}$$

where σ is the electrical conductivity of tissue (S/m), which, if assumed constant, can be eliminated from the equation, and φ is the electric potential (V). The electric field E was obtained as follows:

$$E = -\nabla \varphi \tag{2}$$

In the case of an infinite-length electrode (1D problem), the electrical potential is only a function of the radial coordinate r (see Figure 1B). If we consider that σ is constant (homogeneous tissue), Equation (1) can be stated as follows:

$$\frac{\partial \varphi}{\partial r} \left(r \frac{\partial \varphi}{\partial r} \right) = 0 \tag{3}$$

which is subject to the boundary conditions

$$\varphi(r_i) = V_i \tag{4}$$

$$\varphi(r_o) = 0 \tag{5}$$

where V_i is the voltage applied to the cylindrical electrode. From Equation (3) and the two boundary conditions, the solution can be stated as follows:

$$\varphi(r) = \frac{-V_i}{\ln\left(\frac{r_o}{r_i}\right)} [\ln(r) - \ln(r_o)] \tag{6}$$

The magnitude of the electrical field vector E is

$$|E(r)| = \frac{1}{r} \frac{V_i}{\ln\left(\frac{r_o}{r_i}\right)} \tag{7}$$

In the case of a finite-length electrode (2D problem), and also considering the fact that σ is constant (homogeneous tissue), the electrical potential φ is assumed to be a function of the radial (r) and axial coordinates (z) (Figure 2A). Equation (1) can be stated as follows:

$$\frac{1}{r} \frac{\partial \varphi}{\partial r} \left(r \frac{\partial \varphi}{\partial r} \right) + \frac{\partial^2 \varphi}{\partial z^2} = 0 \tag{8}$$

which is subject to the following boundary conditions:

$$\varphi(r_i, z) = V_i \quad \text{if } z_1 < z < z_2, z_3 < z < z_4 \text{ and } z_5 < z < z_6 \tag{9}$$

$$\left[\frac{\partial \varphi}{\partial z} \right]_{(r,0)} = 0 \tag{10}$$

$$\left[\frac{\partial \varphi}{\partial z} \right]_{(r,z_0)} = 0 \tag{11}$$

$$\varphi(r_o, z) = 0 \tag{12}$$

$$\left[\frac{\partial \varphi}{\partial r} \right]_{(r_i,z)} = 0 \quad \text{if } z < z_1, z_2 < z < z_3, z_4 < z < z_5 \text{ and } z > z_6 \tag{13}$$

The solution for Equation (8) is very similar to what was previously presented in [12]. In essence, it was obtained through the method of separation of variables, dealing with the nonhomogeneous source term and boundary conditions by Green’s functions. On assuming a cylindrical electrode of finite length z_o , the problem combined boundary conditions on the electrode boundary (of the first and second kind). Since this rules out using the Sturm–Liouville theorem, the problem was decomposed into two different problems, and the principle of superposition was used. The obtained solution allowed us to reproduce

the electric field distribution around the electrode, especially the edge effect characterized by an extremely high gradient around the electrode limits.

$$\varphi_1(r, z) = \sum_{m=1}^{\infty} A_m \cos(\eta_m z) \left[K_0(\eta_m r) - \frac{K_0(\eta_m r_o)}{I_0(\eta_m r_o)} I_0(\eta_m r) \right]$$

where $I_0(\eta_m r)$ and $K_0(\eta_m r)$ are the modified Bessel functions of the first and second kind, respectively, and η_m is the eigenvalue for this problem.

$$\eta_m = \frac{(2m - 1)\pi}{2z_0}$$

and

$$A_m = \frac{2I_0(\eta_m r_o)}{z_0 \eta_m} \frac{\chi V_T + \vartheta V_o}{K_0(\eta_m r_i) I_0(\eta_m r_o) - K_0(\eta_m r_o) I_0(\eta_m r_i)}$$

$$\chi = \sin(\eta_m z_1) + \sin(\eta_m z_3) - \sin(\eta_m z_2) + \sin(\eta_m z_5) - \sin(\eta_m z_4) + \sin(\eta_m z_0) - \sin(\eta_m z_6)$$

$$\vartheta = \sin(\eta_m z_2) - \sin(\eta_m z_1) + \sin(\eta_m z_4) - \sin(\eta_m z_3) + \sin(\eta_m z_6) - \sin(\eta_m z_5)$$

$$\varphi_2(r, z) = \sum_{n=1}^{\infty} C_n \cos(\eta_n z) \left[K_0(\eta_n r) - \frac{K_0(\eta_n r_o)}{I_0(\eta_n r_o)} I_0(\eta_n r) \right]$$

where

$$C_n = \frac{-2I_0(\eta_n r_o)}{z_0 \eta_n} \frac{\sum_{m=1}^{\infty} A_m \eta_m \left[K_1(\eta_m r_i) + \frac{K_0(\eta_m r_i) I_1(\eta_m r_o)}{I_0(\eta_m r_o)} \right]}{[K_1(\eta_n r_i) I_0(\eta_n r_o) + K_0(\eta_n r_i) I_1(\eta_n r_o)]} \Psi$$

and

$$\begin{aligned} \Psi = & \left[\frac{\sin((\eta_m + \eta_n)z_1)}{2(\eta_m + \eta_n)} + \frac{\sin((\eta_m - \eta_n)z_1)}{2(\eta_m - \eta_n)} \right] \\ & + \left[\frac{\sin((\eta_m + \eta_n)z_3)}{2(\eta_m + \eta_n)} + \frac{\sin((\eta_m - \eta_n)z_3)}{2(\eta_m - \eta_n)} \right] - \left[\frac{\sin((\eta_m + \eta_n)z_2)}{2(\eta_m + \eta_n)} + \frac{\sin((\eta_m - \eta_n)z_2)}{2(\eta_m - \eta_n)} \right] \\ & + \left[\frac{\sin((\eta_m + \eta_n)z_5)}{2(\eta_m + \eta_n)} + \frac{\sin((\eta_m - \eta_n)z_5)}{2(\eta_m - \eta_n)} \right] - \left[\frac{\sin((\eta_m + \eta_n)z_4)}{2(\eta_m + \eta_n)} + \frac{\sin((\eta_m - \eta_n)z_4)}{2(\eta_m - \eta_n)} \right] \\ & + \left[\frac{\sin((\eta_m + \eta_n)z_0)}{2(\eta_m + \eta_n)} + \frac{\sin((\eta_m - \eta_n)z_0)}{2(\eta_m - \eta_n)} \right] - \left[\frac{\sin((\eta_m + \eta_n)z_6)}{2(\eta_m + \eta_n)} + \frac{\sin((\eta_m - \eta_n)z_6)}{2(\eta_m - \eta_n)} \right] \end{aligned}$$

In the special case of $\eta_m = \eta_n$,

$$\frac{\sin((\eta_m - \eta_n)z)}{2(\eta_m - \eta_n)} \rightarrow \frac{z}{2}$$

From superposition, $\varphi = \varphi_1 + \varphi_2$. The magnitude of the electric field vector E is calculated as follows:

$$|E(r, z)| = \sqrt{\left(\frac{\partial \varphi}{\partial r}\right)^2 + \left(\frac{\partial \varphi}{\partial z}\right)^2} \tag{14}$$

From the analytical solutions shown in Equations (7) and (14), and using MATLAB R2013b (MathWorks, Natick, MA, USA), we computed the values of $|E|$ along the z axis at certain distances from the electrode surface, using the code provided in the Supplementary Materials. $|E|$ was constant along the z axis in the case of infinite length since only the r coordinate is relevant. We chose the distances that allow for mapping the relevant area in sufficient detail in terms of clinical application, specifically, every 1 mm deep in the tissue up to 10 mm. In order to plot the analytical solutions, we set 25 V on the active electrode. Note that this value is not important in the context of our objective of comparing the cases of finite length vs. infinite length.

3. Results

3.1. Verification

Although the solution is purely analytical, and there is therefore no spatial discretization (meshing), the outer radial dimension (r_o in Figure 2A) must be large enough to avoid boundary effects. We conducted convergence tests by increasing r_o from 60 to 150 mm while keeping the other parameters fixed, such as the insulated section length ($S = 30$ mm), the active section length ($L = 20$ mm), $r_i = 0.75$ mm, and $z_0 = 210$ mm, and assessed the electric field values at $r = 1.75$ mm near the center and end of the electrode length. Figure 3 shows the progress of the electric field at two locations (center $z = 25$ mm or $\bar{z} = L/2$, and end $z = 15$ mm or $\bar{z} = 0$) and at 1 mm from the electrode surface as the outer radial dimension r_o increased from 60 to 150 mm. The difference between the results for $r_o = 120$ mm and $r_o = 150$ mm was only 0.27%. For this reason, an outer dimension of 120 mm seems to be suitable.

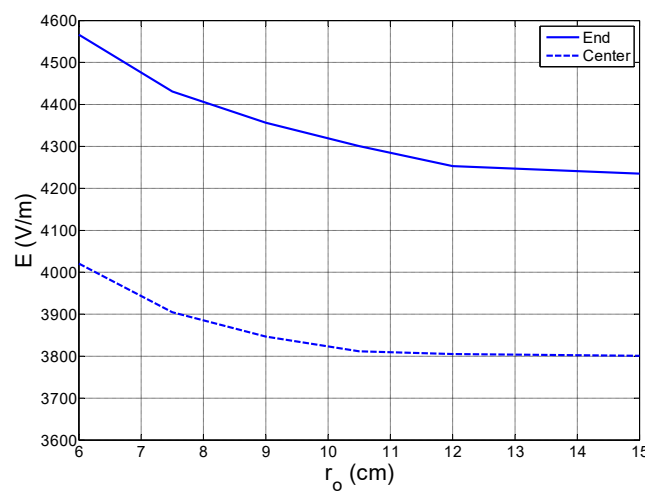


Figure 3. The magnitude of the electric field vector $|E|$ computed at the center ($r = 1.75$ mm, $z = 25$ mm) and the end ($r = 1.75$ mm, $z = 15$ mm) of the electrode for different outer radial dimensions r_o . The case with $S = 30$ mm, $L = 20$ mm, $r_i = 0.75$ mm and $z_0 = 210$ mm.

3.2. Comparison between Infinite and Finite Length

Figure 4 shows the difference in the magnitude of the electric field vector $|E|$ along the lines parallel to the axis of the electrode, comparing the 2D and 1D cases, both on its surface and at distances of 1, 2, and 3 mm from said surface. Note that the 2D case corresponds to the cylindrical electrode of finite length, while the 1D case corresponds to the cylindrical electrode of infinite length (in the graph, $L = 30$ mm, $S = 20$ mm, $r_i = 0.75$ mm, $r_o = 120$ mm, and $z_0 = 210$ mm). As can be observed in the finite-length case, oscillations appear in the solution corresponding to the surface of the electrode ($r = 0.75$ mm). Bessel functions are obtained through power series, which may require too many terms for high precision. Some authors have recognized the limited accuracy inherent in the series calculation of Bessel functions [15]. In our case, the imprecision in the calculation is reflected in the electrode surface showing oscillations and is probably due to the high ratio r_o/r_i in our solution, we have Bessel function terms with the argument $\eta_m(r_i)$ and others in which the argument is

$$\eta_m(r_o)$$

As the argument $\eta_m(r_i)$ is very small compared with $\eta_m(r_o)$, we need too many eigenvalues (in our computation, we used as many as 380 eigenvalues, because using a larger number leads to overflow) to account for Bessel functions evaluated at $\eta_m(r_i)$, but that also includes Bessel functions of large argument $\eta_m(r_o)$, which are usually imprecise. The imprecisions are cumulative by the fact that the solution for φ_2 already carries the errors accumulated from the calculation of φ_1 . The oscillations are caused by the inability of

the computer to have sufficient precision in the calculation of eigenvector functions (Bessel functions), and thus they should not be considered.

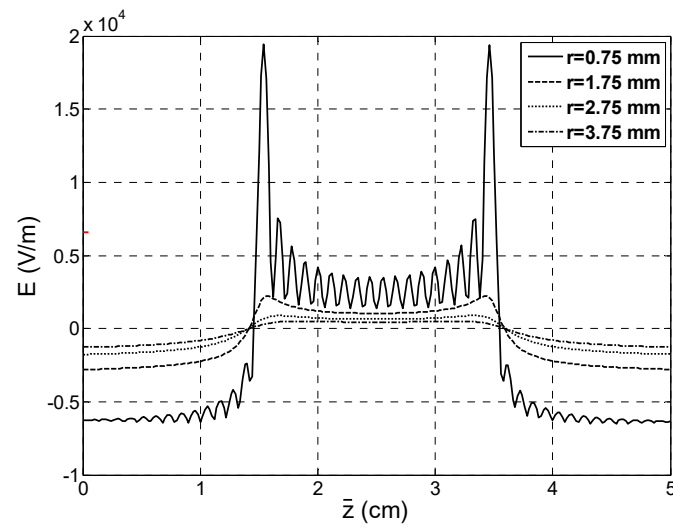


Figure 4. The difference in the magnitude of the electric field vector $|E|$ between 2D and 1D models ($2D - 1D$), along the lines parallel to the axis of an electrode, both on its surface and at distances of 1, 2, and 3 mm from said surface ($L = 30$ mm, $S = 20$ mm, $r_i = 0.75$ mm, $r_o = 120$ mm, and $z_0 = 210$ mm).

The most noticeable finding is that the electric field value computed for the cylindrical electrode of finite length (2D) is always higher than that computed for the electrode of infinite length (1D), especially in the vicinity of the electrode (<1 mm distance) and at the edges, i.e., the joining points with the plastic. The electric field computed for the cylindrical electrode of finite length (2D) is lower than that computed for the electrode of infinite length (1D) outside the tissue zone corresponding with the electrode length ($z < 15$ mm and $z > 35$ mm). We are only interested in the electric field induced in the tissue around the finite-length electrode and in how different it is from that of the infinite-length electrode. In this regard, the differences are smaller for remote points. For instance, at the midpoint of the electrode, the 2D solution provides an electric field that is ~ 250 V/cm higher than the 1D solution just on the electrode surface ($r = 0.75$ mm), while the difference is lower than 100 V/cm at 2 mm distance ($r \geq 2.75$ mm). Although the difference seems to be much more dramatic at the edges, this is only important on the electrode surface (difference up to 1800 V/cm), since the difference remains around 100 V/cm for distances beyond 2 mm. In other words, the edge effect in electric terms, which cannot be reproduced using the 1D solution, seems to be quite important at the points very close to the electrode surface (≤ 1 mm). Meanwhile, the electric field predictions for distant points (≥ 2 mm) conducted with the 1D model would have an underestimation that is more or less constant along the length of the electrode. The real impact of this underestimation would depend on the specific medical application. For instance, in the simulated case of 25 V, it is ~ 100 V/cm. Since there is a direct relation between the applied voltage and the induced electric field, the underestimation could be up to 8000 V/cm in the case of the applied voltage of 2 kV, which is a typical value used during irreversible electroporation for tissue ablation.

3.3. Variation in Electrode Parameters

Figure 5 shows the magnitude of the electric field vector $|E|$ along the lines parallel to the axis of the electrode, both on its surface ($r = r_i$) and at distances of 1, 2, and 3 mm from said surface, as well as for four values of electrode radius r_i : 0.5, 0.75, 1, and 1.25 mm. The rest of the parameters were kept constant. The 2D solution (finite-length electrode) is plotted in blue, and the 1D (infinite-length electrode) is plotted in red. As expected, both 1D and 2D solutions showed $|E|$ values lower as the electrode radius increased. Moreover, the difference between the 2D and 1D solution was also smaller as the electrode radius

increased. For example, at the center of the electrode ($z = 25 \text{ mm}$ or $\bar{z} = L/2$), and just on its surface ($r = r_i$), the $|E|$ value computed with the 2D solution was 35 V/cm higher than 1D for $r_i = 0.5 \text{ mm}$, and it reduced to 15 V/cm for $r_i = 1.25 \text{ mm}$. The general electric behavior described in the previous section (Section 3.2) was identical when the electrode radius changed, i.e., the edge effect was marked for short distances ($\leq 1 \text{ mm}$), while for medium distances ($\geq 2 \text{ mm}$), the difference between 1D and 2D solutions was more or less constant along the electrode length.

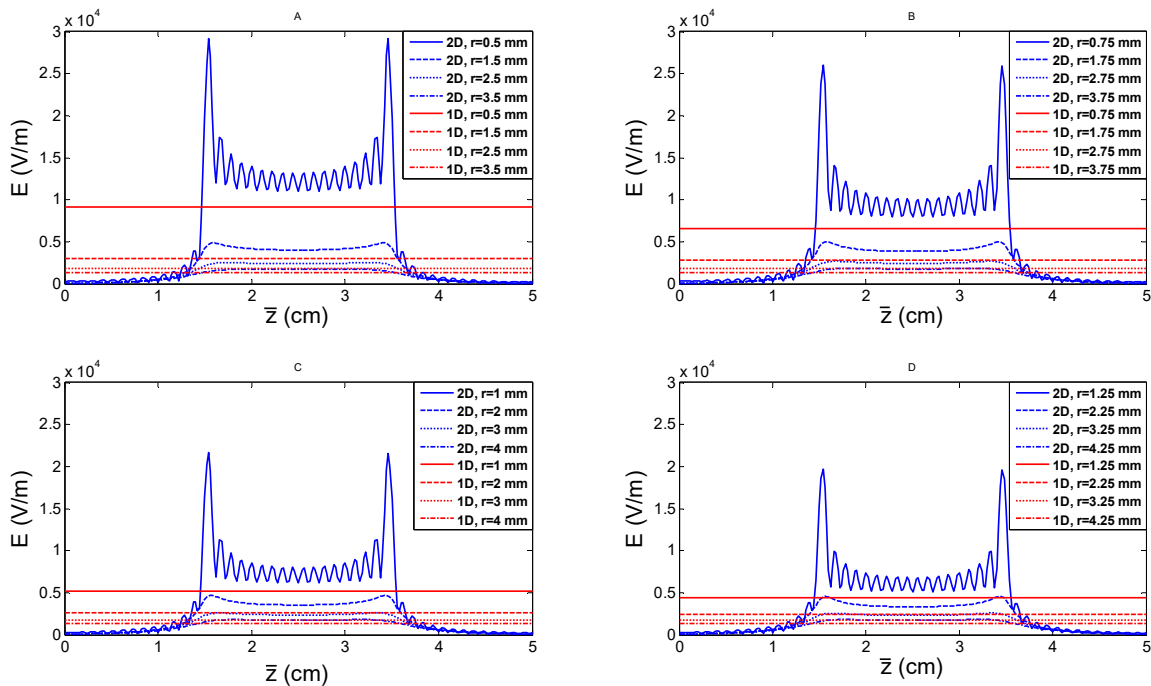


Figure 5. The magnitude of the electric field vector $|E|$ along lines parallel to the axis of an electrode, both on its surface and at distances of 1, 2, and 3 mm from said surface. Graphs are for four values of electrode radius r_i : 0.5 mm (A), 0.75 mm (B), 1 mm (C), and 1.25 mm (D) ($L = 20 \text{ mm}$, $S = 30 \text{ mm}$, $r_o = 120 \text{ mm}$, and $z_0 = 210 \text{ mm}$).

Figure 6 shows the magnitude of the electric field vector $|E|$ along the lines parallel to the axis of the electrode, both on its surface ($r = r_i$), and at distances of 1, 2, and 3 mm from said surface. Graphs show the results for four different lengths of the active electrode L (in case of finite length): 10 mm (A), 20 mm (B), 30 mm (C), and 40 mm (D). The rest of the parameters were kept constant. Similar to what occurred with the electrode radius, the $|E|$ values were increasingly smaller as the electrode length increased. Interestingly, as the length of the electrode increased, the difference between the 2D and 1D solution reduced in the central zone of the electrode.

Figure 7 shows the magnitude of the electric field vector $|E|$ along the lines parallel to the axis of the electrode. The lines represent $|E|$ values, at the surface ($r = r_i$), and at distances of 1, 2, and 3 mm from said surface, as well as for four different lengths of the insulation of the electrode (in case of finite length), namely 10, 20, 30, and 40 mm, while keeping the rest of the parameters constant. In this case, the difference between the 1D and 2D solution was minimal, with a very slight increase in the $|E|$ values as the length of the plastic portion increased.

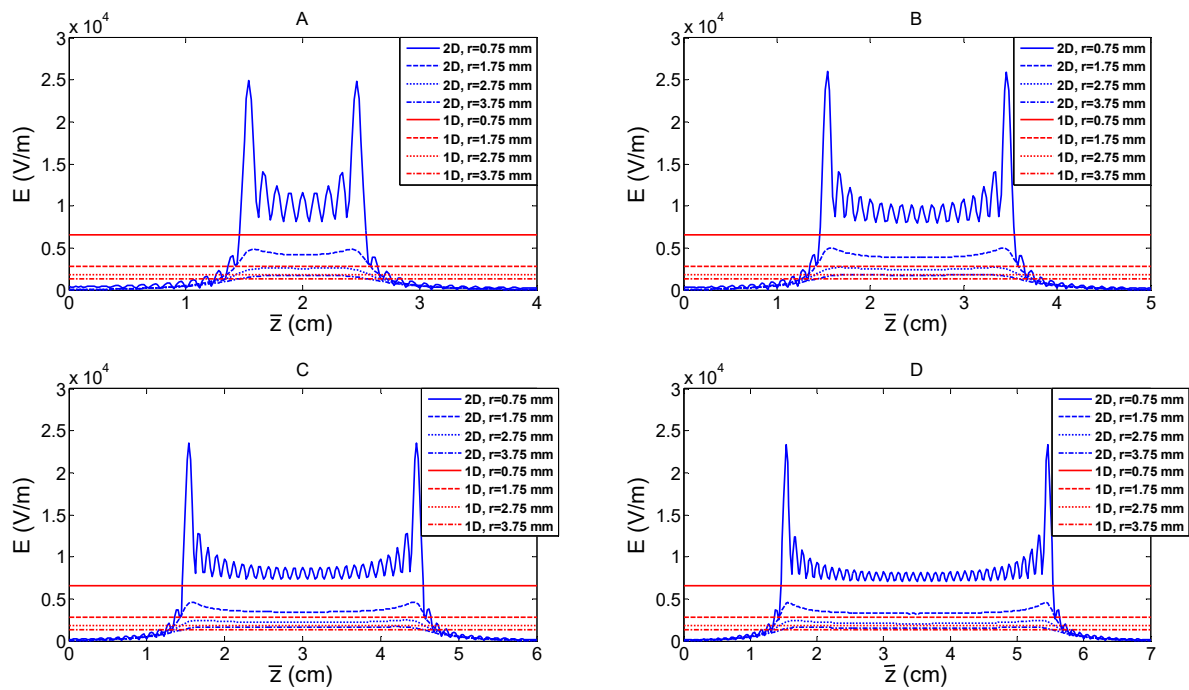


Figure 6. The magnitude of the electric field vector $|E|$ along the lines parallel to the axis of an electrode 1.5 mm in diameter ($r_i = 0.75$ mm), both on its surface and at distances of 1, 2, and 3 mm from said surface. Graphs are for four lengths of the electrode L (in case of finite length): 10 mm (A), 20 mm (B), 30 mm (C), and 40 mm (D) ($r_i = 0.75$ mm, $L = 20$ mm, $S = 30$ mm, $r_o = 120$ mm, and $z_0 = 210$ mm).

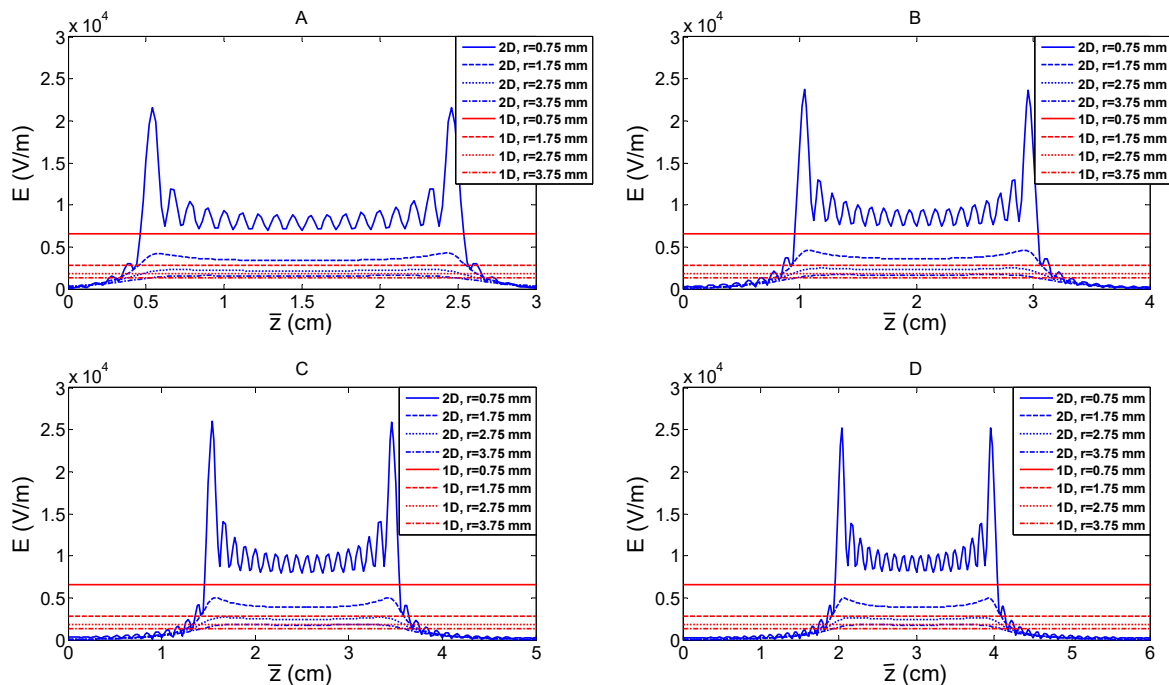


Figure 7. The magnitude of the electric field vector $|E|$ along lines parallel to the axis of an electrode 1.5 mm in diameter ($r_i = 0.75$ mm), both on its surface and at distances of 1, 2, and 3 mm from said surface. Each graph is for a different length of the insulated part of the electrode (in case of finite length): 10 mm (A), 20 mm (B), 30 mm (C), and 40 mm (D) ($r_i = 0.75$ mm, $L = 20$ mm, $r_o = 120$ mm and $z_0 = 210$ mm).

4. Discussion

The mathematical modeling of the electrical behavior of cylindrical electrodes allows for the prediction of the values of the electric field induced in biological media (such as biological tissue and cell suspension) in response to an applied voltage, which is undoubtedly very important in biomedical applications such as stimulation [16], electroporation [17], dielectrophoresis [18,19], and impedance measurement [20]. In these applications, electrodes with very different geometries are used, such as parallel-facing electrodes, coplanar electrodes, and needle-type electrodes. The latter are cylindrical electrodes that are characterized by having a length much greater than their diameter, and they are found in numerous medical devices, specifically housed in plastic catheter-type structures. Considered this way, the electrode is a piece of metal defined by its external diameter and its length. In the monopolar mode, an electrical voltage is applied between the electrode and a large (~150 cm) patch-type electrode that is located at a distant point (e.g., on the patient's skin), which causes the electric field distribution in the biological tissue around the cylindrical electrode. Needle-shaped electrodes are also widely used in medicine, and although they have a sharp tip, they have a usually very small diameter compared with their length, which allows us to assume that the central area behaves like a cylindrical electrode. The electrical behavior around the tip is complex and represents a mathematical singularity in the case of an ideal sharp tip. It is true that there are also some electrodes, such as those used in radiofrequency cardiac ablation, which are cylindrical in shape but end with a hemispherical tip. In these cases, the induced electric field around the cylindrical zone will follow the behavior described in our study, while the electric field around the spherical zone is described in our previous works [21,22] and only numerical solutions could predict the behavior at the interface between both geometries.

The cylindrical structure of these electrodes suggests an axial symmetry that can significantly simplify the mathematical resolution of the problem by assuming a one-dimensional problem, at least when the surrounding tissue is homogeneous. While the problem is very simple to solve for the case of an electrode of infinite length [3], the analytical solution is relatively complex for the case of an electrode of finite length, as occurs in reality [12].

However, when the tissue is not homogeneous, and one wants to solve the problem in the presence of layers of different types of tissue, for example, it is much more complicated to use a 1D model. In that case, a 2D model can be used, assuming that the electrode has an infinite length (see Figure 1C), thus reducing a 3D model to a 2D one. It is precisely in these cases that it becomes necessary to know how different the prediction of the electric field will be due to the assumption of an infinite length. This was the reason for this study.

In our study, we compared the analytical solutions of the magnitude of the electric field vector $|E|$ for the cases of infinite and finite lengths of a cylindrical electrode surrounded by biological tissue. The comparison was performed for different dimensions of the electrode in ranges corresponding to the electrodes used in different clinical procedures, which provides information with direct application for researchers working on stimulation and electroporation. In both cases, the electric field distribution is the most important parameter, since in the first case, it causes the excitation of the cell [23], while in the second case, it induces the formation of pores through the cell membrane [24].

Our main finding confirms what has already been observed by other authors [10,12]: The infinite-length model does not allow us to reproduce the edge effect, i.e., the extremely high values of the electric field induced in the tissue located just at the ends of the finite-length electrode (joining zones with the plastic). However, these "hot spots" in electrical terms, which also appear on the periphery of circular disk-type electrodes [25], appear to be only relevant in areas very close to the electrode (<1 mm for the specific conditions considered in our study, i.e., electrode dimensions and applied voltage value). In other words, for points further away (≥ 2 mm), the electric field distribution is more or less constant along the length of the electrode.

It is also worth noting that the solution that considers the finite length always provides greater electric field values than the one that assumes an infinite length, and this is the case for a wide range of electrode diameter and electrode length values. The practical implication of this is that a simple model that assumes an infinite length will always underestimate the values of the electric field induced in the tissue, even in the center of the electrode, so the biophysical effect (e.g., stimulation or electroporation) will be greater in reality than that predicted with the model.

The difference between both models (finite vs. infinite length) gradually becomes smaller as we move away from the surface of the electrode, and the length of the electrode increases (for the central points). Our results therefore suggest that a simple model based on an electrode of infinite length can predict the electric field values relatively well, both at tissue points located in the middle zone of the electrode and at a sufficient distance from its surface. The prediction with this simple model will be even better the longer the electrode is. However, note that the appropriateness of the prediction using a model based on infinite length is highly dependent on the specific medical procedure to be modeled. This is because the differences in absolute terms of the electric field are proportional to the applied voltage, and while for 25 V, the difference is around 100 V/cm at a 2 mm distance from the electrode, it can be up to 8000 V/cm. cm for a 2 kV application, which is a very high electric field value and must not be ignored at all. This suggests that analytical solutions like the one presented here should serve as tools to be used by researchers in order to verify how reasonable the prediction of the electric field would be in the case of opting for a simple geometry model that assumes an electrode with infinite length. In other words, it cannot be assumed that a model based on an electrode with infinite length can be valid in all circumstances in terms of providing solutions similar to those provided with a finite-length model.

An important limitation of our study is that the comparison between both models was performed assuming homogeneous tissue. Although the presence of tissue layers will surely alter the electric field distribution [6], it is reasonable to assume that the qualitative conclusions of our study in terms of the differences between both solutions will remain valid, at least for spatial tissue configurations based on the layers oriented in the direction of the electrode axis. Finally, another technical limitation was the impossibility of eliminating oscillations in the solution of the electric field immediately on the surface of the electrode. This limitation solely results from the programming intended for plotting, while the analytical solution obtained is correct and complete, which can also serve to verify numerical solution codes.

5. Conclusions

Our study shows the first comparison in terms of the electrical field between mathematical models for cylindrical electrodes with infinite vs. finite length. Our study provides a complete analytical solution available so that researchers can adapt it in the future to the specific dimensions of their electrodes in order to assess the prediction error that would entail using an approximation based on a model that assumes an electrode of infinite length. For the specific values simulated here, i.e., for the dimensions of a cylindrical electrode commonly used in electroporation and electrical stimulation, the electric field distribution induced in the tissue when the real physical situation is oversimplified by assuming an infinite length of the electrode can become substantially different from the case of infinite length, not only in the edges of the electrode and in close locations (<1 mm) but also even in the central area and at distances greater than 2 mm. Our work presents the analytical solutions for both cases (finite and infinite length), which, despite the oscillations derived from computational limitations, could be used by researchers involved in electric field modeling in biological tissues, in order to quantify the possible error generated with simple models in geometric terms that assume infinite length.

Supplementary Materials: The following supporting information can be downloaded at: <https://www.mdpi.com/article/10.3390/math11214447/s1>. The file “CodeCalculationElectricField.m” is the code developed in MATLAB R2013b for the calculation of the electric field distribution in a region shown in Figure 2, mathematically stated with Equations (8)–(13) and solved using the method for the separation of variables as described in this paper.

Author Contributions: Conceptualization, R.R.-M. and E.B.; methodology, R.R.-M. and E.B.; software, R.R.-M.; validation, R.R.-M.; formal analysis, R.R.-M. and E.B.; writing—review and editing, R.R.-M. and E.B.; funding acquisition, E.B. All authors have read and agreed to the published version of the manuscript.

Funding: This research was funded by the Spanish Ministerio de Ciencia e Innovación/Agencia Estatal de Investigación (MCIN/AEI/10.13039/501100011033) with Grant Number PID2022-136273OB-C31.

Data Availability Statement: No data supporting reported results is needed. Results are not experimental and numerical results can be obtained compiling the code included in Supplementary Materials.

Conflicts of Interest: The authors declare no conflict of interest.

References

1. Boido, D.; Kapetis, D.; Gnatkovsky, V.; Pastori, C.; Galbardi, B.; Sartori, I.; Tassi, L.; Cardinale, F.; Francione, S.; de Curtis, M. Stimulus-evoked potentials contribute to map the epileptogenic zone during stereo-EEG presurgical monitoring. *Hum. Brain Mapp.* **2014**, *35*, 4267–4281. [[CrossRef](#)]
2. González-Suárez, A.; Irastorza, R.M.; Deane, S.; O’Brien, B.; O’Halloran, M.; Elahi, A. Full torso and limited-domain computer models for epicardial pulsed electric field ablation. *Comput. Methods Programs Biomed.* **2022**, *221*, 106886. [[CrossRef](#)]
3. Haemmerich, D.; Chachati, L.; Wright, A.; Mahvi, D.; Lee, F.; Webster, J. Hepatic radiofrequency ablation with internally cooled probes: Effect of coolant temperature on lesion size. *IEEE Trans. Biomed. Eng.* **2003**, *50*, 493–500. [[CrossRef](#)]
4. Collavini, S.; Fernández-Corazza, M.; Oddo, S.; Princich, J.P.; Kochen, S.; Muravchik, C.H. Improvements on spatial coverage and focality of deep brain stimulation in pre-surgical epilepsy mapping. *J. Neural Eng.* **2021**, *18*, 046004. [[CrossRef](#)]
5. Molina, J.A.L.; Rivera, M.J.; Berjano, E. Analytical transient-time solution for temperature in non perfused tissue during radiofrequency ablation. *Appl. Math. Model.* **2017**, *42*, 618–635. [[CrossRef](#)]
6. González-Suárez, A.; O’Brien, B.; O’halloran, M.; Elahi, A. Pulsed Electric Field Ablation of Epicardial Autonomic Ganglia: Computer Analysis of Monopolar Electric Field across the Tissues Involved. *Bioengineering* **2022**, *9*, 731. [[CrossRef](#)]
7. González-Suárez, A.; Pérez, J.J.; O’Brien, B.; Elahi, A. In silico modelling to assess the electrical and thermal disturbance provoked by a metal intracoronary stent during epicardial pulsed electric field ablation. *J. Cardiovasc. Dev. Dis.* **2022**, *9*, 458. [[CrossRef](#)]
8. Dev, S.; Dhar, D.; Krassowska, W. Electric field of a six-needle array electrode used in drug and DNA delivery in vivo: Analytical versus numerical solution. *IEEE Trans. Biomed. Eng.* **2003**, *50*, 1296–1300. [[CrossRef](#)]
9. Pupo, A.E.B.; Reyes, J.B.; Cabrales, L.E.B.; Cabrales, J.M.B. Analytical and numerical solutions of the potential and electric field generated by different electrode arrays in a tumor tissue under electrotherapy. *Biomed. Eng. Online* **2011**, *10*, 85. [[CrossRef](#)]
10. McRury, I.D.; Panescu, D.; Mitchell, M.A.; Haines, D.E. Nonuniform heating during radiofrequency catheter ablation with long electrodes. *Circulation* **1997**, *96*, 4057–4064. [[CrossRef](#)]
11. Romero-Méndez, R.; Berjano, E. An analytical solution for radiofrequency ablation with a cooled cylindrical electrode. *Math. Probl. Eng.* **2017**, *2017*, 9021616. [[CrossRef](#)]
12. Romero-Méndez, R.; Pérez-Gutiérrez, F.G.; Oviedo-Tolentino, F.; Berjano, E. Analytical solution for electrical problem forced by a finite-length needle electrode: Implications in electrostimulation. *Math. Probl. Eng.* **2019**, *2019*, 2404818. [[CrossRef](#)]
13. Čorović, S.; Pavlin, M.; Miklavčič, D. Analytical and numerical quantification and comparison of the local electric field in the tissue for different electrode configurations. *Biomed. Eng. Online* **2007**, *6*, 37. [[CrossRef](#)] [[PubMed](#)]
14. Sel, D.; Mazeres, S.; Teissie, J.; Miklavcic, D. Finite-element modeling of needle electrodes in tissue from the perspective of frequent model computation. *IEEE Trans. Biomed. Eng.* **2003**, *50*, 1221–1232. [[CrossRef](#)]
15. Paris, R. High-precision evaluation of the Bessel functions via Hadamard series. *J. Comput. Appl. Math.* **2009**, *224*, 84–100. [[CrossRef](#)]
16. Wei, X.F.; Grill, W.M. Current density distributions, field distributions and impedance analysis of segmented deep brain stimulation electrodes. *J. Neural Eng.* **2005**, *2*, 139–147. [[CrossRef](#)]
17. Corovic, S.; Lackovic, I.; Sustaric, P.; Sustar, T.; Rodic, T.; Miklavcic, D. Modeling of electric field distribution in tissues during electroporation. *Biomed. Eng. Online* **2013**, *12*, 16. [[CrossRef](#)]
18. Gauthier, V.; Bolopion, A.; Gauthier, M. Analytical formulation of the electric field induced by electrode arrays: Towards automated dielectrophoretic cell sorting. *Micromachines* **2017**, *8*, 253. [[CrossRef](#)]
19. Sun, T.; Morgan, H.; Green, N.G. Analytical solutions of ac electrokinetics in interdigitated electrode arrays: Electric field, dielectrophoretic and traveling-wave dielectrophoretic forces. *Phys. Rev. E Stat. Nonlinear Soft Matter Phys.* **2007**, *76*, 046610. [[CrossRef](#)]

20. Sun, T.; Green, N.; Gawad, S.; Morgan, H. Analytical electric field and sensitivity analysis for two microfluidic impedance cytometer designs. *IET Nanobiotechnol.* **2007**, *1*, 69–79. [[CrossRef](#)]
21. Molina, J.A.L.; Rivera, M.J.; Berjano, E. Electrical-thermal analytical modeling of monopolar RF thermal ablation of biological tissues: Determining the circumstances under which tissue temperature reaches a steady state. *Math. Biosci. Eng.* **2016**, *13*, 281–301. [[CrossRef](#)]
22. Rivera, M.; Molina, J.; Trujillo, M.; Berjano, E. Theoretical modeling of RF ablation with internally cooled electrodes: Comparative study of different thermal boundary conditions at the electrode-tissue interface. *Math. Biosci. Eng.* **2009**, *6*, 611–627. [[CrossRef](#)]
23. Meng, S.; Rouabhia, M.; Zhang, Z. Electrical stimulation and cellular behaviors in electric field in biomedical research. *Materials* **2021**, *15*, 165. [[CrossRef](#)]
24. Napotnik, T.B.; Polajžer, T.; Miklavčič, D. Cell death due to electroporation—A review. *Bioelectrochemistry* **2021**, *141*, 107871. [[CrossRef](#)]
25. Wiley, J.D.; Webster, J.G. Analysis and control of the current distribution under circular dispersive electrodes. *IEEE Trans. Biomed. Eng.* **1982**, *29*, 381–385. [[CrossRef](#)]

Disclaimer/Publisher’s Note: The statements, opinions and data contained in all publications are solely those of the individual author(s) and contributor(s) and not of MDPI and/or the editor(s). MDPI and/or the editor(s) disclaim responsibility for any injury to people or property resulting from any ideas, methods, instructions or products referred to in the content.